Contribution from the IBM T. J. Watson Research Center,
Yorktown Heights, New York 10598

# Preparation Using the Metal Atom Technique and Properties of Nickel Microparticles

B. A. SCOTT,* R. M. PLECENIK, G. S. CARGILL III, T. R. McGUIRE, and S. R. HERD

*Received August 3, 1979*

The structural, morphological, and magnetic properties of small nickel particles prepared by the metal atom technique from toluene, $SF_6$, and xenon matrices at 77 K are reported. X-ray scattering and electron microscopy measurements indicate that the smallest particles are obtained from toluene matrices. Particle size depends upon the initial nickel concentration in the toluene matrix, reaching ~16-Å average diameter for the highest concentrations studied. The microcrystals prepared from toluene are surrounded by a thin amorphous organic layer, comprising up to 10 wt % of the total sample, due to solvent decomposition on melt-down and subsequent heating to room temperature. The particles are dispersed within larger agglomerates >100 Å in diameter. Microcrystallites obtained from $SF_6$ and xenon are larger. The xenon-prepared nickel is relatively pure, typically ~100 Å in size, and exhibits faceting. Toluene-prepared powders display ferromagnetic behavior with magnetic moments ~40% that of bulk Ni for the largest microcrystallites and paramagnetism for the smallest (metal clusters). The role of matrix solvent in the nucleation and growth of clusters and microcrystallites is also examined and discussed in view of current interest in their catalytic properties.

## Introduction

Cocondensation and subsequent reaction of metal atoms and organic molecules have been used in recent years as a synthetic method for the preparation of many new organometallic compounds.[1-3] Such reactions may occur during deposition and/or subsequent warm-up. Alternatively, the organic matrix can react with clusters containing several, or many, metal atoms. At the low temperatures employed (typically 78 K), metal oligomerization is favored over the formation of an activated organometallic species, particularly if the organic substrate lacks highly reactive substituents or functional groups. Recently, Klabunde and co-workers[4-7] have taken advantage of this tendency toward oligomerization to produce active nickel particles with catalytic activity or selectivity for various hydrogenation, disproportionation, and isomerization reactions.[8] For example, nickel particles prepared by cocondensation of Ni atoms in pentane matrices are more reactive than Raney nickel in olefin hydrogenations.[6] Since there is a competition between Ni-cluster growth and Ni-cluster reaction with pentane,[5] considerable amounts of hydrocarbon fragments can be incorporated into the catalysts during preparation, consequently modifying their surface properties. Thus, the potential exists for designing catalytic systems having selectivity and activity for specific processes depending upon the matrix solvent used in the preparation. Moreover, the quenching of metal atoms from the vapor state into either inert or interacting matrices provides a new route to other types of metastable phases having unusual structures and properties. For this reason, we have prepared and investigated the properties of very small nickel particles prepared by the "metal atom" synthetic approach.

Evidence based on infrared measurements[9] suggests that the codeposition of Ni with arenes and substituted arenes (for Ni:arene $\lesssim$ 1:100) leads to weak $\pi$-complex formation and that the complex is stable to just above the matrix melting temperature, whereupon it decomposes with the formation of small nickel particles.[4] As will be seen, the occurrence of competing reactions at low temperature results in nickel microparticles which have incorporated organic fragments in a special way. On the basis of X-ray diffraction, electron microscopy, and magnetic measurements, we propose a model to describe the structure and morphology of the nickel microparticles precipitated from low-temperature matrices.

## Experimental Section

The nickel microparticles were prepared by evaporation of 99.9% Ni metal (Cerac; −20 mesh) at temperatures just above its melting point (1452 °C) in a metal atom reactor similar to an earlier design.[3] The metal was evaporated from resistively heated, alumina-coated tungsten baskets (Sylvania Emissive Products, CS1002) after outgassing at ~700 °C at a base pressure in the $10^{-5}$-torr range. Approximately 300 mg of metal was evaporated in each run, while ~3–50 g of matrix solvent was used. The toluene matrix solvent (Burdick & Jackson, "Distilled in Glass") was dried ($P_2O_5$) and then degassed in several freeze–thaw cycles prior to cryopumping into the reactor, which was maintained at 78 K by a liquid-$N_2$ bath. The percentage of metal deposited in the matrices was calculated from the weight loss of the evaporated basket and the amount of solvent distilled from a calibrated flask. There is, however, considerable error (±30%) in the quoted values of this parameter because some of the metal deposits on the reactor wall above the matrix. Also, the concentrations calculated in this way are average values because the emission of metal atoms from the hot crucible follows roughly a cosine angular distribution law. Upon completion of the evaporation, the liquid-nitrogen bath was removed and the matrix allowed to melt (~−96 °C). It then warmed to room temperature, and the resulting metal powder was removed under a blanket of inert gas by using Schlenk-tube techniques. The solid was isolated by distilling off the solvent under vacuum, since the material was too fine to be filtered. It was then stored in an inert-atmosphere box (<1 ppm of $O_2$ and $H_2O$).

In addition to the experiments in toluene, a number of runs were made by using $SF_6$ and Xe matrices, as these were expected to be completely inert toward the highly reactive nickel atoms. Since these matrix materials are gases at room temperature, the nickel could not be isolated by the usual Schlenk-tube techniques. Instead, they were magnetically drawn into an isolation tube and transferred to the drybox.

Magnetic moment measurements were carried out as a function of magnetic field by using a Faraday-type balance. The samples were sealed into special glass vials in the drybox because of their pyrophoricity. We have found that materials produced from matrices in which the nickel concentration exceeds ~5 wt % are not visibly pyrophoric. Since the samples had to receive air exposure during handling and measurement in the X-ray and electron microscopy experiments, the more detailed studies were performed on samples prepared from the more concentrated matrices.

Standard X-ray measurements were carried out on a Philips diffractometer, while a 6-kW rotating-anode Rigaku Denki instrument was used for both large-angle (LAS) and small-angle (SAS) X-ray

(1) P. L. Timms and T. W. Turney, *Adv. Organomet. Chem.*, **15**, 53 (1977).
(2) M. J. McGlinchey and P. S. Skell in "Cryochemistry", Martin Moskovits and Geoffrey A. Ozin, Eds., Wiley, New York, 1976, pp 167–94.
(3) K. J. Klabunde, *Acc. Chem. Res.*, **8**, 393 (1975).
(4) K. J. Klabunde, H. F. Efner, T. O. Murdock, and R. Ropple, *J. Am. Chem. Soc.*, **98**, 1021 (1976).
(5) S. C. Davis and K. J. Klabunde, *J. Am. Chem. Soc.*, **100**, 5973 (1978).
(6) K. J. Klabunde, S. C. Davis, H. Hattori, and Y. Tanaka, *J. Catal.*, **54**, 254 (1978).
(7) K. J. Klabunde, D. Ralston, R. Zoellner, H. Hattori, and Y. Tanaka, *J. Catal.*, **55**, 213 (1978).
(8) There is an extensive literature on metal cluster and supported metal catalysts: E. L. Muetterties, T. N. Rhodin, Elliot Band, C. F. Brucker, and W. R. Pretzer, *Chem. Rev.*, **79**, 91 (1979); A. K. Smith and J. M. Basset, *J. Mol. Catal.*, **2**, 229 (1977); Charles L. Thomas, "Catalytic Processes and Proven Catalysts", Academic Press, New York and London, 1970.
(9) H. F. Efner, D. E. Tevault, W. B. Fox, and R. R. Smardzewski, *J. Organomet. Chem.*, **146**, 45 (1978).

0020-1669/80/1319-1252$01.00/0 

**Table I**

| No. | Matrix | Ni Conc. At. % | %Ni | %C | %H | %O* | %S | %F | Moles H / Moles C | |
|---|---|---|---|---|---|---|---|---|---|---|
| 15 | toluene | 0.4 | 71.54 | 5.77 | 1.17 | 21.52 | - | - | 2.43 | |
| 14 | toluene | 2.4 | 82.80 | 3.82 | 0.27 | 13.11 | - | - | 0.85 | |
| 11 | toluene | 3.7 | 84.08 | 2.87 | 0.42 | 12.63 | - | - | 1.75 | |
| 13 | toluene | 8.3 | 87.84 | 4.09 | 1.59 | 6.48 | - | - | 4.66 | |
| 12 | toluene | 13.7 | 88.85 | 4.10 | 0.37 | 6.68 | - | - | 1.08 | |
| 26A | toluene | 2.7 | 80.71 | 4.66 | 0.73 | 13.90 | - | - | 1.88 | |
| 26B | toluene | 2.7 | 92.03 | 1.85 | 0.35 | 5.77 | - | - | 2.27 | 26A heated to 700°C |
| 29 | $SF_6$ | 4.8 | 89.76 | 1.13 | 0.50 | 2.39 | 1.38 | 4.84 | - | unexposed |
| 30 | $SF_6$ | 3.6 | 78.79 | 0.73 | 0.76 | 16.97 | 1.07 | 1.68 | - | exposed to ambient |
| 31A | $SF_6$ | 5.4 | 90.64 | 0.59 | 0.37 | ~6.70 | 0.70 | $\lesssim$1.0 | - | unexposed |
| 31B | $SF_6$ | 5.4 | 77.79 | 1.73 | 1.05 | $\approx$18.0 | 0.43 | <1.0 | - | 31A exposed to ambient |
| 27 | Xe | 3.3 | 97.11 | <0.7 | <0.2 | $\approx$2.0 | - | - | - | unexposed |
| 28 | Xe | 2.9 | 87.60 | - | - | $\approx$12.4 | - | - | - | exposed to ambient |

*By difference. The oxygen content has also been confirmed by ESCA analysis (Ref. 26).

scattering studies. For these measurements, about 300 mg of the as-prepared material was compacted in a specially constructed sample holder to form a self-supporting disk of 2.5-cm diameter and 0.05-cm thickness. Measurements were made with Ag K$\alpha$ radiation ($\lambda$ = 0.561 Å) from the line focus of the rotating-anode generator, a computer-controlled diffractometer, and an intrinsic germanium detector. Scattered intensities were measured in a symmetrical transmission configuration with 0.1° steps for scattering angles 2$\theta$ from 3 to 70°. Between 2000 and 9000 counts were accumulated at each angle.

For the electron microscope studies, the Ni powders were ultrasonically dispersed in ethyl alcohol and a drop of the solution was placed on a standard carbon-covered EM grid on filter paper. After most of the solution had drained off, the thinnest clumps of Ni particles were investigated by transmission electron microscopy and diffraction using a Philips EM301 instrument.

## Experimental Results

**Structural and Morphological Studies.** Table I contains a compilation of the experimental results on a series of nickel samples precipitated from toluene, $SF_6$, and xenon. X-ray diffractometer patterns on several of the nickel powders, precipitated at different concentrations from toluene matrices, are presented in Figure 1. Only the (111) and (200) reflections are shown because the higher angle reflections obtained with the standard diffractometer are broadened almost beyond detection. It is obvious from these initial results that a considerable fraction of each specimen is crystalline, with the strongly broadened reflections indicative of microcrystallinity. It should be noted that Figure 1 is intended to illustrate relative trends only because the smaller particles, which are most prevalent in samples prepared at lower metal concentration, are more highly oxidized and do not contribute to the line broadening. Therefore, the qualitative trends of Figure 1 actually overestimate the particle size for the low Ni concentration samples. For example, application of the Scherrer equation[10] to the diffraction spectra of Figure 1 leads respectively to average crystallite sizes of ~20 and 40 Å for the 0.4% and 12% samples. These estimates are at least a

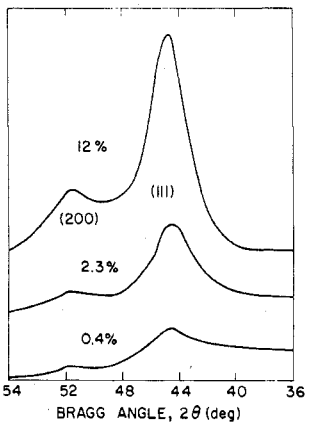


**Figure 1.** X-ray diffraction patterns (Cu K$\alpha$ radiation) obtained from nickel precipitated from toluene matrices. The initial concentration of nickel in the matrices is given in mol %. Only the (111) and (200) reflections are shown.

factor of 2 larger than the values obtained by direct calculation of the interference function, as will be discussed in the next section for a high concentration of metal-in-matrix sample. It is clear, however, from the chemical analysis shown in Table I, that the powders are impure, although the lattice constant calculated from the X-ray patterns is very close to that of the bulk metal. The detailed compositional data will be discussed in a subsequent section.

Extensive X-ray scattering experiments were made on an air-stable nickel sample prepared from a toluene matrix in which the initial Ni concentration was 8.3 mol % (no. 13, Table I). The measurements were corrected for air scattering, Compton scattering, and angle-dependent polarization, irradiated volume, and absorption factors.[11] The measured absorption coefficient for Ag K$\alpha$ radiation was $\mu t$ = 1.28. Normalization to electron units was carried out by the high-

(10) B. D. Cullity, "Elements of X-ray Diffraction", Addison-Wesley, Reading, Mass., 1956, p 99.

(11) C. N. J. Wagner in "Liquid Metals", S. Z. Bear, Ed., Marcel Dekker, New York, 1972, p 257.

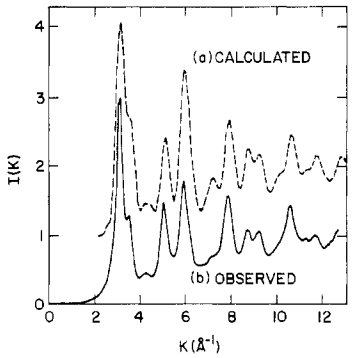


**Figure 2.** Interference functions (a) calculated by assuming 16-Å diameter microcrystals and (b) obtained experimentally for sample no. 13 (Table I).

angle method,[11] treating the sample as if it contained only nickel. The experimentally obtained interference function $I(K)$ shown in Figure 2 was calculated from the normalized scattered intensity $I_{eu}(K)$ by using eq 1, where $K = 4\pi(\sin\theta)/\lambda$ and $f(K)$ is the atomic scattering factor for nickel.

$$I(K) = I_{eu}(K)/f(K)^2 \quad (1)$$

The calculated interference function for this sample was very similar to those calculated for small fccub crystals,[12] and further fccub microcrystal interference functions were calculated for closer comparison with the experimental data. The Debye equation[13] (eq 2) was used, where $r_{ij}$ is the distance

$$I_0(K) = 1 + \frac{1}{N}\sum_{i\neq j}(\sin Kr_{ij})/Kr_{ij} \quad (2)$$

between lattice sites i and j within the microcrystal of Ni atoms. Values of $r_{ij}$ were calculated for fccub microcrystals of nearly spherical shape having diameters of 14, 16, and 20 Å containing 135, 201, and 321 atoms, respectively. The resulting interference functions calculated with eq 2 were modified by a Debye–Waller-type factor to incorporate effects of thermal vibrations and possible random static displacements of atoms from the ideal lattice sites.[13]

$$I(K) = I_0(K)\exp(-\langle u^2\rangle K^2) + [1 - \exp(-\langle u^2\rangle K^2)] \quad (3)$$

An interference function calculated with eq 2 and 3 for 16-Å diameter fccub microcrystals with lattice parameter $a = a_{Ni}$ = 3.5171 Å and $\langle u^2\rangle^{1/2}$ = 0.13 Å is compared with the experimental result in Figure 2. The calculated and measured functions are very similar. The main differences are that the shoulder at 2.8 Å$^{-1}$, corresponding to the (200) Bragg reflection, and the peak at 6 Å$^{-1}$, the (311) and (222) Bragg reflections, are about 30% stronger in the model $I(K)$ than the corresponding features in the experimental interference function.

The lattice parameter used in the calculation was the same as that for bulk nickel, but $\langle u^2\rangle^{1/2}$ is nearly 50% larger than that expected for thermal vibrations at 300 K for bulk nickel.[14] The larger value of $\langle u^2\rangle^{1/2}$ was needed to reduce the amplitude of structure in the model $I(K)$ at larger $K$ values to the experimentally observed level. Since measurements were made only at room temperature, it could not be determined whether the large $\langle u^2\rangle^{1/2}$ was caused by static displacements or by vibrational amplitudes of atoms in the small crystals being larger than those of bulk nickel, i.e., a lowered Debye temperature. Static displacements may result from surface coatings on the small crystals. The very large surface-to-volume ratios for such particles may also alter their average vibrational properties. Although the model interference function for 16-Å diameter fccub microcrystals reproduces the overall experimental peak widths, amplitudes, and positions much better than model functions for either 12- or 20-Å diameter microcrystals, the present values do not rule out a distribution of microcrystal sizes in this range.

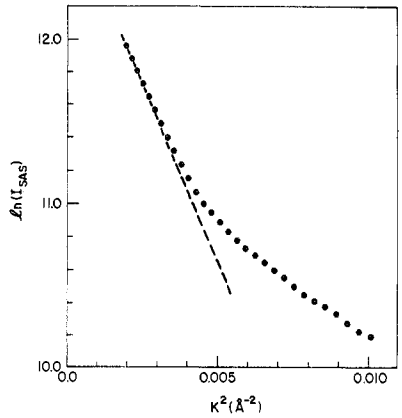


**Figure 3.** Small-angle scattering for sample no. 13 (Table I) plotted as logarithm of the intensity vs. $K^2$. The dashed line indicates the limiting slope corresponding to 100-Å diameter scattering centers.

Because of the much smaller scattering factors and concentrations of H, C, and O compared with those of nickel, the scattering pattern provides no information about their distribution in the powders. However, the success of modeling the scattering pattern with fccub microcrystals having the bulk-nickel lattice parameter indicates that most of the nickel is contained in such microcrystals and that there are probably few bulk sites occupied by these lighter elements. The other elements may be present as an amorphous matrix containing the nickel microcrystals or as a surface coating on the microcrystals, as will subsequently be discussed.

Small-angle scattering measurements were made with the same sample used for the LAS measurements. The SAS measurements also employed Ag K$\alpha$ radiation, with a four-slit SAS goniometer. Results of the SAS measurements, after correction for background and slit-length smearing,[15] are shown in Figure 3. The SAS is very intense for $2\theta < 1°$. The decrease of intensity with increasing scattering angle is much more rapid than expected for SAS from 16-Å diameter scatters, i.e., if the SAS were being produced by the individual microcrystals. The initial slope of ln ($I_{SAS}$) vs. $K^2$ is consistent with scattering by regions of about 100-Å diameter, and the slope of the curve at $K = 0$ may be larger than in the experimental range, indicating the presence of even larger particles. The continuous curvature of the scattering curve with increasing angle indicates that a range of smaller scattering sizes is present.[16]

Although there appears to be a considerable difference between the microcrystalline sizes determined by the LAS and SAS methods, the electron micrographs shown in Figures 4 and 5 indicate that the two methods actually give complementary results. In Figure 4A,B are shown dark-field electron micrographs of Ni particles prepared from 2.4% and 13.7% nickel in toluene, respectively. Here, microparticles ~10–20 Å in size can be observed within larger agglomerates 50–150 Å in diameter. The agglomerates are more readily perceived in the $SF_6$-deposited material shown in Figure 5A,B, where

(12) G. S. Cargill III, *J. Appl. Phys.*, **41**, 12 (1970).
(13) C. N. J. Wagner, T. B. Light, N. C. Halder, and W. E. Lukens, *J. Appl. Phys.*, **39**, 3690 (1968).
(14) H. Morimoto and H. Sakata, *J. Phys. Soc. Jpn.*, **17**, 136 (1962).
(15) P. W. Schmidt, *Acta Crystallogr.*, **19**, 938 (1965).
(16) A. Guinier and G. Fournet, "Small-Angle Scattering of X-Rays", Wiley, New York, 1955, p 113.

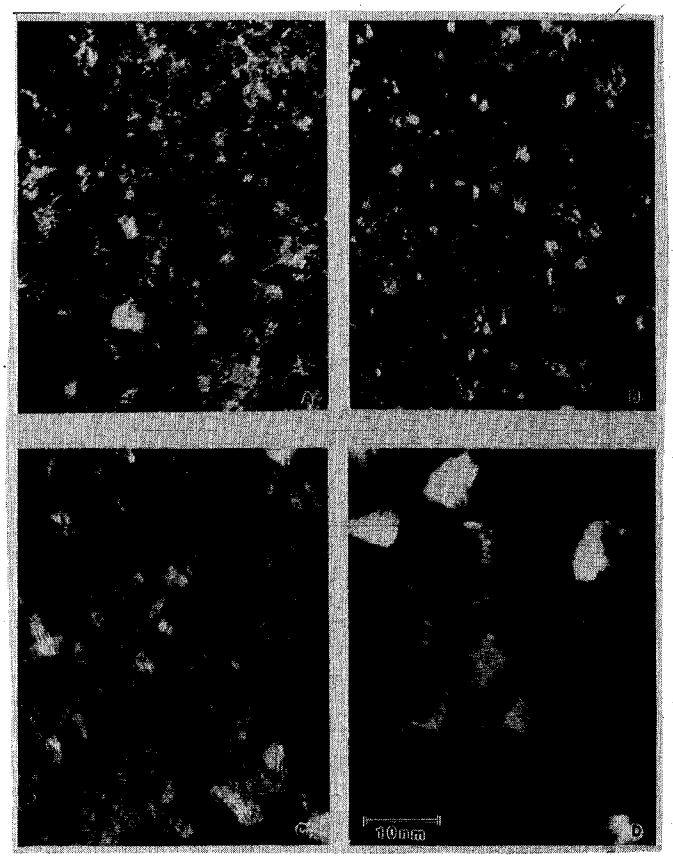


**Figure 4.** Ni (111) dark-field electron micrographs of nickel particles obtained under the following deposition conditions: (a) 2.4% Ni in toluene; (b) 13.7% Ni in toluene; (c) 5.4% Ni in $SF_6$; (d) 2.9% Ni in Xe. Magnification $2 \times 10^6$.

they are linked in a beadlike fashion, probably because of magnetic interactions between them. Thus, both LAS and SAS results are consistent with the electron micrographs. The characteristic size of 16 Å obtained in the LAS from sample no. 13 corresponds to coherent scattering from individual microcrystals, but the range of larger sizes indicated by the SAS corresponds to the dimensions of the agglomerates containing the microcrystals.

Three size ranges were measured from the micrographs depending on the matrix in which the Ni was dispersed. The smallest grain size of 10–20 Å was observed for the toluene matrices. On the basis of the dark- and light-field imaging behavior, it can be deduced that the particles are separated by an amorphous region of organic material and/or oxide. There appears to be more of the amorphous material in samples obtained from matrices having lower Ni concentrations, as shown by qualitative comparison of representative Ni (111) dark-field micrographs in Figure 4A,B. A medium grain size of 20–50 Å was found for Ni from a $SF_6$ matrix (no. 31; Figure 4C), and large 100-Å crystallographically shaped particles were obtained from the xenon matrix (no. 28; Figure 4D). For these samples there is also a notable absence, of course, of the amorphous organic layer, although it is believed that the particles are coated with a thin amorphous NiO skin.

Typical bright- and dark-field images of the $SF_6$- and xenon-matrix Ni particles are shown for comparison at a somewhat lower magnification in Figure 5. The electron diffraction pattern of $SF_6$-prepared Ni particles (no. 29 and 31) showed the presence of crystalline NiO. These lines were not observed in toluene or xenon samples. Although the electron diffraction patterns are essentially of randomly oriented particles, there is a preferred [100] orientation present for samples no. 12 (toluene) and no. 28 (xenon) for which no

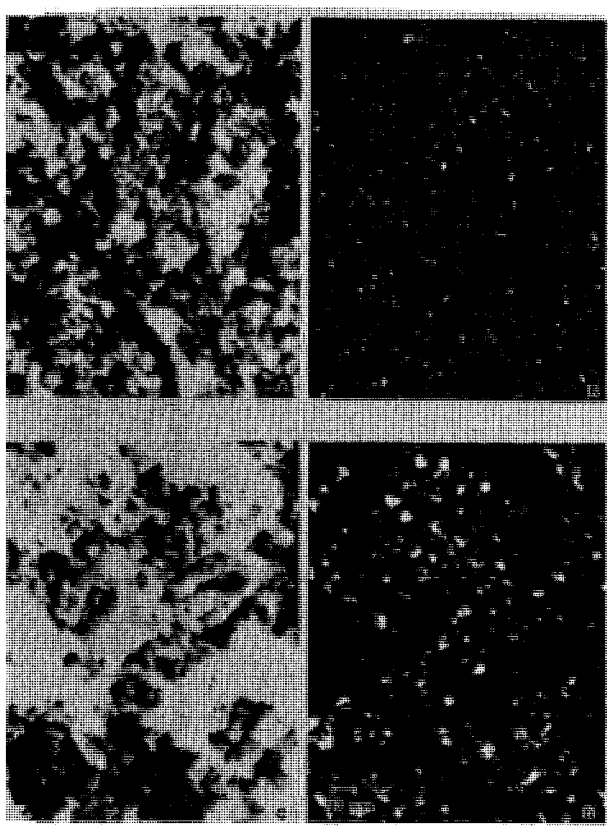

**Figure 5.** Comparison of $SF_6$ (no. 31) and Xe (no. 28) matrix depositions. $SF_6$ (5.4% Ni): (a) bright field; (b) Ni (111) dark field. Xe (2.9% Ni): (c) bright field; (d) Ni (111) dark field. Magnification $4 \times 10^5$.

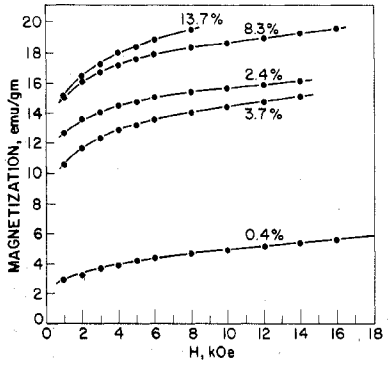


**Figure 6.** Room-temperature magnetization vs. applied magnetic field ($H$) for a series of Ni powders prepared from the indicated initial concentrations (mol %) in toluene matrices.

explanation exists at present. More diffraction work is necessary to determine the significance of the [100] texture. Arrangement of particles in chainlike configurations, as in Figure 5A,B for $SF_6$, was also frequently observed.

**Magnetic Properties.** The magnetization ($M$) of nickel precipitated from toluene depends very strongly on its initial concentration in the matrix, as shown in the room-temperature data of Figure 6. The behavior appears to be ferromagnetic, and $M$ eventually saturates at high magnetic fields, even for the lowest concentration. The largest moments observed are reduced considerably in comparison with that for pure nickel at room temperature (54 emu/g). The temperature dependence of the magnetization for a sample prepared from the most concentrated matrix (no. 12; 13.7%) is shown in Figure 7. There are several features of the magnetic data for this sample that are of significance. First, the field dependence of the magnetization as shown in Figures 6 and 7 indicates

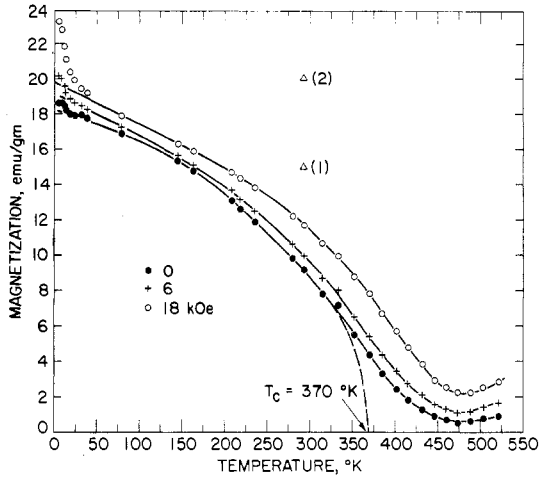


**Figure 7.** Temperature dependence of the magnetization for a sample prepared from a 13.7 mol % Ni/toluene matrix (sample no. 12). The indicated Curie temperature, $T_C$ = 370 K, was obtained by an extrapolation procedure.[18] Triangles represent the room-temperature magnetization obtained on return to room temperature from heating the sample in the first run, (1), and after reheating and annealing at 500 K for 2 h, (2).

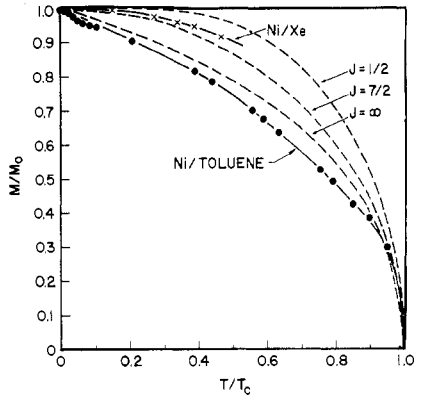


**Figure 8.** Reduced magnetic moment $M/M_0$ for Ni/toluene (sample no. 12) and Ni/Xe (sample no. 27) vs. reduced temperature $T/T_C$. The 4.2 K value was taken for $M_0$. $T_C$ = 370 K and $T_C$(Ni) were used for the toluene and xenon samples, respectively. The dotted curves correspond to calculated Brillouin functions for the indicated $J$ values.

a relatively slow approach to saturation. Second, the $M$ vs. $T$ plots do not exhibit typical Brillouin function behavior.[17] Attempts to fit the data of Figure 7 to such an expression using a Curie temperature $T_C$ = 370 K[18] are shown in Figure 8. Very poor agreement is obtained for the expected[17] total angular momentum $J = {}^1/_2$, while the best fit occurs for $J = \infty$, i.e., the classical case. Even here the agreement is far from satisfactory. These observations hold for all samples prepared from toluene matrices, with the difference between theory and experiment becoming worse with decreasing nickel concentration in the matrices. The results for xenon-prepared materials are, however, much closer to the expected nickel $J = {}^1/_2$ quantum case and would improve further if the assumed $T_C = T_C$(Ni) is relaxed. Since $T_C$ is expected to be lower than $T_C$(Ni), the effect of a lower $T_C$ for Xe would be to shift the experimental curve toward the calculated $J = {}^1/_2$ Brillouin function in Figure 8. Although the particle size averages ~100 Å, much less than the dimensions of a magnetic domain, the

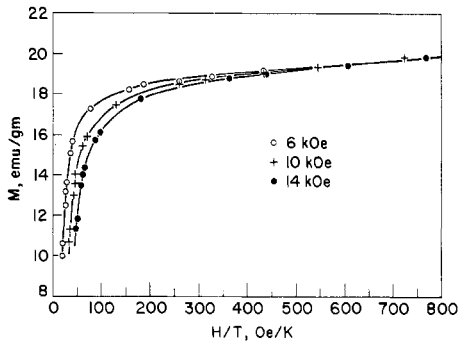


**Figure 9.** Magnetization vs. $H/T$ for sample no. 12 (13.7% Ni in toluene).

particles obtained from xenon can interact more directly since there is no intervening organic phase.

The data of Figure 7 indicate that the magnetization does not reach zero at the extrapolated[18] Curie point, nor at temperatures up to 150 K higher. In fact, $M$ increases as temperature reaches the 450–500 K range and on remeasurement after cooling to room temperature is found to have increased as shown by points (1) and (2) in Figure 7. This is clearly related to the loss of organic material from the sample. The process already begins at a measurable rate at temperatures above 350 K and after temperature cycling always results in a higher magnetization even after correcting for the weight change of the sample due to the material loss.[19] We believe that the increase in magnetization is caused by an enhancement in interparticle coupling as organic surface layers on the microparticles are removed on heating. However, as will subsequently be shown, sintering and grain growth begin to dominate only as this process is taken to its extreme at considerably higher temperatures than utilized in the magnetic studies (>500 °C).

Superparamagnetism, not ferromagnetism, would be expected for isolated nickel particles as small as those produced here (~16 Å for one of the most concentrated matrix samples studied). Figure 9 shows a plot of $M$ vs. $H/T$ for sample no. 12. It is clear that the curves do not superimpose for the different magnetic field strengths, as would be expected for superparamagnetism, especially in the low $H/T$ region where the measurement is most sensitive. These results suggest that the particles are not isolated; that is, they are close enough to one another for magnetic coupling interactions to occur between them. This is consistent with the previous magnetic data and the electron micrographs which show agglomeration of the microparticles into large clumps ≳100 Å and the arrangement of these agglomerates into necklace-like chains. Such behavior has been observed previously in ferromagnetic metals deposited as smokes by evaporation into an inert gas.[20]

Since the nickel particles produced from the most dilute matrices are pyrophoric, X-ray scattering experiments could not be performed on these samples. Therefore, magnetic measurements provide the only information concerning their state of aggregation. In contrast to preparations from the most concentrated matrices, where metal clustering on deposition is evidenced by the formation of a black matrix, in the dilute case the metal atoms form a red-brown complex with the toluene solvent molecules. Figure 10 shows the temperature dependence (solid curve) of the magnetization of the nickel

(17) L. F. Bates, "Modern Magnetism", 4th ed., Cambridge University Press, Cambridge, England, 1963, pp 279–317.

(18) This value was obtained from plots of $M^2$ vs. $H/M$ by extrapolating the high-temperature data to $H/M$ = 0 and finding the temperature at which the intercept becomes zero.

(19) Note that although the sample capsules are tightly closed and glued, decomposition products can be released through the seal if the internal pressure is high enough. However, since the magnetic measurements were carried out in a He atmosphere of 25 torr, there is no chance of contamination by the ambient atmosphere.

(20) K. Kimoto, Y. Kamiya, M. Nonoyama, and R. Uyeda, *Oyo Butsuri*, **2**, 702 (1963); A. Tasaki, S. Tomiya, S. Iida, N. Wada, and R. Uyeda, *ibid.*, **4**, 707 (1965).

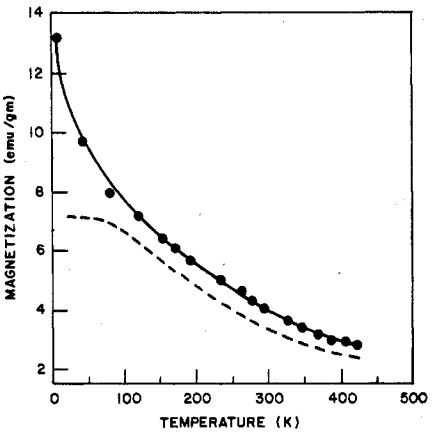


**Figure 10.** Magnetization vs. temperature for sample no. 15 (0.4% Ni) (solid curve). The dashed curve corresponds to the magnetization due to the ferromagnetic "impurity" component obtained from the Honda–Owen slopes as discussed in the text.

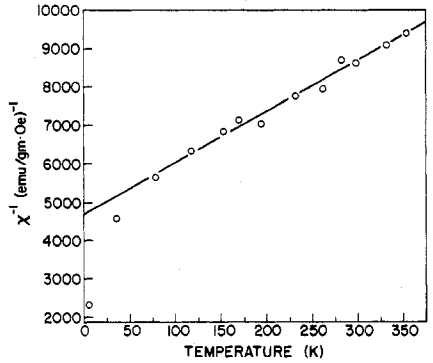


**Figure 11.** The paramagnetic part ($\chi^{-1}$) of the susceptibility for sample no. 15 (0.4% Ni) vs. temperature. The linear slope gives $\mu \simeq 5\ \mu_B$ for the average magnetic moment.

precipitated on melt-down of the matrix under these conditions (0.4% concentration; no. 15, Table I). The increasing magnetization with decreasing temperature suggests paramagnetic behavior; however, if the actual susceptibilities are plotted against $[H]^{-1}$ by using the method due to Honda and Owen,[21] a considerable amount of ferromagnetic "impurity" is found. The "impurity" contribution to the total magnetization is plotted in Figure 10 (dotted curve) where it is seen to contribute the major portion to the total moment at temperatures above 50 K. The difference between the total bulk susceptibility curve and the ferromagnetic "impurity" part is the actual paramagnetic susceptibility, obtained at each temperature from the Honda–Owen intercept. These values are plotted as $\chi^{-1}$ vs. temperature in Figure 11. From the slope of this plot, we obtain a molar Curie constant $C_M = 4.42$ cm$^3$ K, assuming the sample is composed entirely of nickel.

The value $C_M = 4.42$ cm$^3$ K corresponds to a magnetic moment $\mu_{eff} = 5.9$ or $\sim 5\ \mu_B$/mol. This is very high for nickel in any of its most common oxidation states and suggests that the paramagnetic component present in samples produced from very dilute matrices consists of clusters containing a small number of exchange-coupled Ni atoms.[22] Since the clusters must contain bound organic fragments and oxygen, it is likely that nickel is present in a variety of oxidation states (probably all low). The susceptibility becomes augmented because the exchange-enhanced magnetic moment enters as the square in the Curie constant ($C_M = N_0\mu_{eff}^2/3k$) while Avogadro's number $N_0$ is reduced only linearly by the number of atoms making up the cluster. If it assumed that all of the nickel atoms are divalent, the number of atoms in the cluster would be $5.9^2/2.83^2 \approx 4$, where $\mu_{eff}(Ni^{2+}) = 2.83$. However, this value cannot be taken too literally considering the assumptions involved in the calculation and the method used to extract the paramagnetic contribution to the total susceptibility.

Thus, the nickel microparticles obtained from the very lowest nickel-matrix concentrations are really mixtures exhibiting a range of magnetic behavior. The smallest "particles" in the mixture are isolated clusters containing a small number of nickel atoms bound with organic fragments. These show no magnetic ordering at all but a Curie-like susceptibility with an exchange-enhanced moment. Larger particles are also present: the ferromagnetic "impurities", with sizes ranging up to the largest observed in the high concentration runs, ~20 Å. Their magnetic behavior is suggestive of a system composed of ferromagnetic particles displaying a spectrum of Curie temperatures (i.e., a superposition of Brillouin or Langevin functions, each with a different $T_C$) correlated to its particle-size distribution.

## Discussion

Structural and electron microscopic studies of nickel powders prepared from highly concentrated toluene matrices suggest that the metal initially precipitates from the matrix in the form of small microcrystals having the fccub Ni structure with virtually no change in lattice constant. Calculations of the X-ray scattering intensity suggest that most of the nickel is incorporated into the microcrystals. Thus, it can be surmised that the organic fragments detected in the chemical analysis (Table I) are largely on the surfaces of the particles or coexist as a separate phase. There are several observations that provide evidence for the former conclusion. If the organic fragments are tightly bound within the microcrystals (and because of the nature of the binding leave the fccub lattice parameter unchanged), most of the carbon should remain on slow heating to high temperatures. On the other hand, if the organic fragments are bound mostly to the microcrystallite surfaces, or are present as a separate phase, most should be removed on heating. A nickel sample produced from a 2.7% Ni/toluene matrix was slowly heated to 700 °C under vacuum with a loss of nearly 60% of its non-Ni content, including oxygen (26A,B, Table I). The carbon-content change is somewhat larger, from 4.66 to 1.85 wt %. An account can be made for almost 80% of the observed weight change by assuming that C, H, and O loss occurs as $CO_2$ and $H_2O$, i.e., that the organic fragments are oxidized by oxygen present in the samples. The resulting solid would have a Ni:C atomic ratio of 10 and an overall composition $Ni_{10}CH_{2.27}O_{2.27}$.

The loss of most of the carbon on high-temperature heating is consistent with its presence as a surface species. Klabunde and co-workers have observed the evolution of $CO_2$, $H_2O$, and other organic products on heating toluene-prepared $Ni/Al_2O_3$ catalysts.[6] At low temperatures the catalysts primarily eliminate toluene, methylcyclohexane, benzene, and $CO_2$, but on warm-up to 600 °C the predominant products are $H_2$, $CH_4$, $CO_2$, and $H_2O$.[6] Sample 26B showed evidence of weight loss still occurring in magnetic measurements at $T_C = 610$ °C, so that not all of the carbonaceous material is removed in the 700 °C heating. Moreover, this Curie temperature is 20 K lower than that of pure Ni, and the saturation magnetization measured at room temperature, $M_S = 45$ emu/g, is 20% smaller. X-ray diffraction patterns of sample 26B showed crystalline material (~1-$\mu$ particles) after calcination under vacuum with no evidence of other phases present. Therefore, the remaining carbon, hydrogen, and oxygen must be in solid solution. It is interesting that the equilibrium solubility of oxygen in Ni is only 0.07 wt %, with carbon exhibiting a somewhat larger value of 0.5 wt .[23] These limits are con-

(21) Reference 17, p 134.
(22) W. C. Muellner and J. S. Kouvel, *AIP Conf. Proc.*, **5**, 487 (1971).

siderably lower than those found in sample 26B after heating. The incorporation of carbon and oxygen into Ni solid solution at concentrations above the equilibrium values is not surprising because the reactants are initially codeposited atomically at low temperatures. Probably, continued heating at even higher temperature would result in an approach to the equilibrium concentrations.

In addition to evidence from X-ray scattering, electron microscopy, and other experiments, there is an even stronger argument for the existence of an amorphous surface layer on the nickel particles from electrical conductivity measurements. Dc experiments on sample no. 13 gave a room-temperature value (four-probe method) $\sigma = 20\ (\Omega\ cm)^{-1}$. We find $\sigma = 10^5\ (\Omega\ cm)^{-1}$ for a pure Ni sample (3–5-$\mu$ particle size) measured under identical conditions. Since such a low value of conductivity cannot be ascribed to the presence of 10–15% impurity as a separate phase, we conclude that each microcrystallite is coated with an amorphous layer having lower conductivity. Assuming that the density of the surface film lies somewhere between that of NiO ($d = 2.4$) and Ni ($d = 8$), we calculate a maximum layer thickness ranging from 2 Å for 10 wt % to 5.5 Å for 25 wt % second-phase component. These values are consistent with an electron tunneling controlled conductivity through the surface layer and with the retention of ferromagnetic properties, since interparticle magnetic coupling could occur across such small thicknesses. The amorphous surface layer probably also contains nickel atoms, although the majority of the metal is incorporated in the fccub microcrystallite core of each particle.

Precipitation of the metal from more dilute matrices results in a greater proportion of the surface phase and lower values of bulk magnetization and Curie temperature. At this extreme in composition, the material can be considered as composed of nickel–organic clusters which are too small and dilute to exhibit any long-range magnetic effects. The clusters are mixed with larger particles to give a range of aggregate sizes and a concomitant range in magnetization and Curie temperature. Note that the net magnetization observed in the most dilute system is just 10–15% that of bulk Ni. Thus, at the lowest dilutions studied, the metal atom technique is probably beginning to approach the limit of minimum particle size that can be attained.

## Summary and Conclusions

The present studies show that nickel microparticles produced under deposition conditions typically used to prepare reactive metal slurries and supported metal catalysts[6,7] are comprised of crystalline cores up to 15–20 Å in diameter covered with an amorphous surface layer containing mostly organic matrix fragments and oxygen. These dimensions are probably close to the upper limit to be expected in the preparation of slurries and catalysts. In fact, particle diameters in this range may be the maximum obtainable by the metal atom technique when matrix solvents such as toluene are used. On the assumption that metal precipitation occurs in the liquid phase due to the oligomerization of metal atom monomers that are weakly bound to the arene, two separate reactions compete on warm-up of the Ni/toluene solution.[5] Initially, small naked metal clusters form and act as nuclei for the growth of the microcrystallites, but with increasing temperature, decomposition of the arene ensues with the rapid accumulation of organic fragments (and scavanged oxygen) around the growing particle. When the microcrystallite reaches some critical size, the buildup of decomposition products impedes further growth. Thus, the process becomes self-limiting. The maximum size depends on many factors, including the matrix reactivity, metal atom concentration, and thermal history of the metal/matrix composite. For Ni/toluene our results suggest that ~20 Å may be the upper limit.

This growth model is consistent with the fact that much larger particles grow from more inert solvents. Larger microparticles were obtained from $SF_6$ (35–50 Å), even though here there is evidence (Table I) that some reaction is occurring. The largest particles (~100 Å) were obtained from xenon matrices. The formation of a decomposition product layer on each crystallite also explains the observation that nickel prepared from dilute matrices are pyrophoric—since these samples have a larger fraction of very small "unprotected" microcrystallites and clusters susceptible to rapid oxidation on exposure to the ambient atmosphere. Moreover, the formation of an amorphous layer implies that catalyst preparation and properties will also depend upon the matrix solvent used, and very special surfaces having specific reactivities could be created by the metal atom method, a result already realized in Klabunde's investigation.[6,7] On the other hand, the preparation of supported microparticles having surfaces that are more nickel-like will probably require extensive hydrogen reduction at high temperatures with a concomitant decline in catalyst surface area.

It should be pointed out at this juncture that very little can be said about the detailed nature of the surface layer itself. Its overall composition, although dependent on initial nickel concentration in the matrix, is influenced also by sample handling and history. For this reason, we do not believe any significance can be attached to the relative compositions of the samples, i.e., for example, that carbon and hydrogen are detected in $SF_6$- and xenon-prepared powders (Table I, samples 27–31) or that sulfur and fluorine were also detected in the former materials, prepared from ostensibly "inert" $SF_6$. In view of the high reactivity of the matrix-prepared Ni in general, it is not surprising that ~10–20 wt % of impurities or decomposition products are always observed despite the precautions taken with the various workup procedures and physical measurements. Detailed analysis is indeed very difficult, and it is our main point only to show that the particles can be considered essentially as relatively pure Ni microcrystallite cores surrounded by amorphous surface layers formed during preparation and exposure of the samples to the atmosphere. Our analysis, then, is that on as-prepared materials and for this reason is related directly to the nature of the particles deposited on a catalyst support, for example.

The results presented here probably apply with little qualification to nickel and other metal particles prepared by codeposition into saturated hydrocarbon matrices.[4-7] As above, the ultimate size of the particles will depend on both the reactivity of the solvent and the preparative conditions. For example, Davis and Klabunde[5] have recently shown that even alkanes are cleaved during the formation of Ni particles from Ni/alkane dispersions at temperatures ~−130 °C. Nonferromagnetic nickel is produced from very dilute Ni/pentane slushes (1:300) while ferromagnetic material is obtained at higher concentrations (1:100). However, if the nickel is allowed to remain in the pentane slush at −130 °C for several hours prior to warming to room temperature, nonferromagnetic particles precipitate with as little as 1:40 excess of pentane. Prolonged exposure and reaction of the nickel clusters formed initially at the melt-down temperature thus leads to the accumulation of solvent decomposition products which limit growth to microparticles having considerably reduced moments and/or only weak interparticle magnetic coupling because of a very thick surface layer (i.e., comparable to our powders produced from the most dilute toluene matrices).

Although we have implicitly assumed that nickel particle growth commences from small clusters formed in the matrix

(23) F. A. Shunk, "Constitution of Binary Alloys", 2nd suppl., McGraw-Hill, New York, 1969, p 550.

liquid just above its melting point, it is likely that many of the nickel atoms are already present in the form of small molecular clusters (2–10 or more atoms) prior to melting. These may form because of surface diffusion of the metal atoms during codeposition or bulk diffusion on matrix warm-up. Ozin and co-workers have extensively investigated these factors in the formation of dimers and higher oligomers of transition metals in inert matrices.[24,25] Vanadium, for example, shows evidence of appreciable dimerization due to surface diffusion in $CH_4$ matrices during deposition at 10–12 K under conditions of quite high dilution[25] ($V:CH_4 = 1.5:1000$). In general, it was found that bulk diffusion becomes important at temperatures around one-third of the matrix melting point.[25] On the basis of this criterion, a large fraction of the nickel atoms must be present in oligomeric form at the melting point of toluene. Since matrix decomposition becomes important only in the liquid phase, and on heating to room temperature, some degree of control of cluster and microcrystallite size might be possible by appropriate choice of solvent to enhance both surface and bulk diffusion rates in the solid during codeposition and subsequent warm-up of the metal/matrix phase.

**Acknowledgment.** The authors wish to thank H. R. Lilienthal, W. E. Krull, and R. Linn for their expert assistance with the magnetic, X-ray, and electrical measurements. We are also grateful to Dr. K. J. Klabunde and Dr. P. L. Timms for informative discussions and suggestions.

**Registry No.** Ni, 7440-02-0.

(24) E. P. Kündig, M. Moskovits and G. A. Ozin, *Nature (London)*, **254**, 503 (1975); R. Busby, W. Klotzbücher, and G. A. Ozin, *J. Am. Chem. Soc.*, **98**, 4013 (1976); G. A. Ozin and H. Huber, *Inorg. Chem.*, **17**, 155 (1978).
(25) W. E. Klotzbücher, S. A. Mitchell, and G. A. Ozin, *Inorg. Chem.*, **16**, 3063 (1977).
(26) R. Johnson, personal communication.

Contribution from the Department of Chemistry, University of Rochester, Rochester, New York 14627

# Exchange Coupling in Copper Dimers with Purine Ligands

D. SONNENFROH and R. W. KREILICK*

*Received September 10, 1979*

The EPR spectra of a series of dimeric copper complexes with purine ligands have been investigated to determine dipolar splittings and exchange energies. The copper atoms in these complexes are coordinated to the nitrogen atoms in the purine rings in each case but have different axial ligands. The metal–metal separations and dipolar couplings are similar in this group of molecules, but there are large differences in the exchange energies. The variation in exchange energy with the nature of the axial ligand can be explained by a mechanism involving mixing of the $d_{z^2}$ and $d_{x^2-y^2}$ orbitals with overlap of the $d_{z^2}$ orbitals of the two copper atoms.

## Introduction

There are a variety of biologically important transition-metal complexes which contain more than one metal atom per molecule. The magnetic properties of such complexes depend on the exchange coupling of the metal atoms. The exchange interaction varies with the separation of the metal atoms, with the relative orientation of the orbitals of the metal atoms, and with the nature of the ligands surrounding the metal atoms.[1] If one considers complexes in which each metal atom has a single electron spin, the Hamiltonian operator describing the Zeeman, hyperfine, dipolar, and exchange interactions is given by eq 1. In this expression the $A_i$'s are the electron–nuclei

$$\mathcal{H} = g\beta HS_z + \sum_i A_i S_{iz} I_{iz} + D[S_z^2 - \tfrac{1}{3}S^2] + E[S_x^2 - S_y^2] + JS_1 \cdot S_2 + S_1 D_e S_2 \quad (1)$$

hyperfine coupling constants, $D$ and $E$ are constants describing the dipolar interaction, $J$ is the isotropic exchange energy, and $D_e$ is the anisotropic exchange energy.[2,3] The anisotropic exchange term arises from spin–orbit coupling, and the magnitude of this term is dependent on the symmetry of the crystal. If the two metal atoms in a copper dimer are located at points A and B, respectively, and the point bisecting the line AB is donated by C, the anisotropic term is zero when C is a center of inversion for the complex.[2] Point C was a center of inversion for all of the complexes reported in this study, and the observed anisotropic splitting of the EPR spectra arises entirely from the dipolar interaction. If the electron spins are considered to be point dipoles, one can obtain an estimate of the separation of metal atoms ($r$) from the dipolar splitting in the EPR spectrum as in eq 2. The point-dipole approximation is an oversimplification for copper complexes and should not give exact distances but does provide a reasonable comparison of changes in electron–electron separations within a series of similar complexes.

$$D = \tfrac{3}{2}(\mu/r^3) \quad (2)$$

The exchange interaction for complexes of this type splits the energy level into singlet and triplet states. The Hamiltonian for the exchange interaction is given by eq 3. The

$$J = \int\int (\psi_a(1))(\psi_b(2))|H_{ex}|(\psi_b(1))(\psi_a(2))\, d\tau_1\, d\tau_2$$

$$H_{ex} = \frac{e^2}{r_{12}} + \frac{Z_a^* Z_b^* e^2}{R} - \frac{Z_b^* e^2}{r_{1b}} - \frac{Z_a^* e^2}{r_{2a}} \quad (3)$$

exchange interaction may result from direct overlap of the metal atoms' d orbitals or may involve orbitals in the coordinated ligands. In cases in which direct overlap of the d orbitals dominates the exchange interaction, the magnitude of this interaction will vary with the separation and orbital orientation of the metal atoms and with the crystal field

(1) G. F. Kokoszka, *Coord. Chem. Rev.*, **5**, 209 (1970); P. F. Richardson and R. W. Kreilick, *J. Phys. Chem.*, **82**, 1149 (1978); P. F. Richardson and R. W. Kreilick, *J. Am. Chem. Soc.*, **99**, 8183 (1977); C. R. Mao and R. W. Kreilick, *Mol. Phys.*, **31**, 1447 (1976).
(2) T. Moriya, *Phys. Rev.*, **120**, 91 (1960).
(3) K. T. McGregor and Z. G. Soos, *Inorg. Chem.*, **15**, 2159 (1976); *J. Chem. Phys.*, **64**, 2506 (1976); K. T. McGregor, D. J. Hodgson, and W. A. Hatfield, *Inorg. Chem.*, **15**, 421 (1976); B. Morosin, R. C. Hughes, and Z. G. Soos, *Acta Crystallogr., Sect. B*, **31**, 762 (1975); K. T. McGregor, D. B. Losee, D. J. Hodgson, and W. E. Hatfield, *Inorg. Chem.*, **13**, 756 (1974).

0020-1669/80/1319-1259$01.00/0 